Supporting Information for:

"Modeling reactive ammonia uptake by secondary organic aerosol in CMAQ: application to continental US"

Shupeng Zhu[1], Jeremy R. Horne[1], Julia Montoya-Aguilera[2], Mallory L. Hinks[2], Sergey A. Nizkorodov[2], and Donald Dabdub[1]

[1]Computational Environmental Sciences Laboratory, Department of Mechanical & Aerospace Engineering, University of California, Irvine, Irvine, CA, 92697-3975, USA

[2]Department of Chemistry, University of California, Irvine, Irvine, CA, 92697-3975, USA

Correspondence to: Donald Dabdub
(ddabdub@uci.edu)

1 Additional tables

Table S1. Definitions of the statistical parameters used in this work. o_i and c_i are the observed and the simulated concentrations at time and location i, respectively. n is the number of data. $\bar{o}$ and $\bar{c}$ are averaged observed and the simulated concentrations, respectively.

Statistic indicator	Definition
Root mean square error (RMSE)	$\sqrt{\frac{1}{n}\sum_{i=1}^{n}(c_i - o_i)^2}$
Correlation	$\frac{\sum_{i=1}^{n}(c_i - \bar{c})(o_i - \bar{o})}{\sqrt{\sum_{i=1}^{n}(c_i - \bar{c})^2}\sqrt{\sum_{i=1}^{n}(o_i - \bar{o})^2}}$
Mean normalised gross bias (MNGB)	$\frac{1}{n}\sum_{i=1}^{n}\frac{o_i - c_i}{c_i}$
Mean normalised gross error (MNGE)	$\frac{1}{n}\sum_{i=1}^{n}\frac{\lvert o_i - c_i\rvert}{c_i}$
Mean fractional bias (MFB)	$\frac{1}{n}\sum_{i=1}^{n}\frac{c_i - o_i}{(c_i + o_i)/2}$
Mean fractional error (MFE)	$\frac{1}{n}\sum_{i=1}^{n}\frac{\lvert\, c_i - o_i\,\rvert}{(c_i + o_i)/2}$

Table S2. Comparison between simulation results for PM_{10} and observations from the AQS network. (Obs. stands for observation; Sim. stands for simulation. Corr. stands for correlation; No. Sites means number of observation site used for statistics.)

Scenario	Period	Obs. mean $\mu g/m^{-3}$	Sim. mean $\mu g/m^{-3}$	RMSE $\mu g/m^{-3}$	Corr. %	MFB %	MFE %	No. Sites
Base	Summer	26.6	28.6	34.5	7.8	14.1	63.0	225
γ=10^{-3}	Summer	26.6	30.4	36.1	7.8	17.8	65.0	225
γ=10^{-4}	Summer	26.6	28.7	34.7	7.8	14.6	63.3	225
γ=10^{-5}	Summer	26.6	28.6	34.5	7.8	14.2	63.0	225
Base	Winter	19.7	16.0	24.3	13.8	-8.8	65.9	229
γ=10^{-3}	Winter	19.7	15.6	24.2	13.9	-10.4	65.6	229
γ=10^{-4}	Winter	19.7	15.9	24.3	13.9	-9.0	65.8	229
γ=10^{-5}	Winter	19.7	16.0	24.3	13.8	-8.8	65.9	229

Table S3. Comparison between base case simulation results for SO_4^{2-} and observations from CSN network. (Obs. stands for observation; Sim. stands for simulation. Corr. stands for correlation; No. Sites means number of observation site used for statistics.)

Period	Obs. mean $\mu g/m^{-3}$	Sim. mean $\mu g/m^{-3}$	RMSE $\mu g/m^{-3}$	Corr. %	MFB %	MFE %	No. Sites
Summer	2.94	3.18	1.75	32.4	12.6	47.2	193
Winter	1.91	1.52	1.06	54.1	-14.9	47.5	193

2 Additional figures

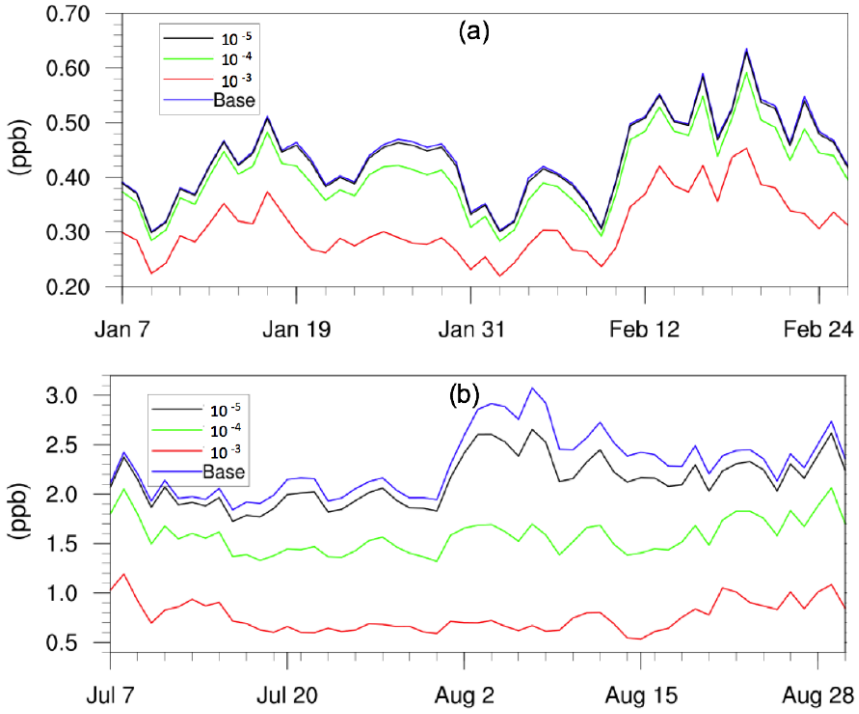

Figure S1. Daily, spatially-averaged NH_3 concentrations for different uptake coefficient scenarios for (a) winter period, and (b) summer period

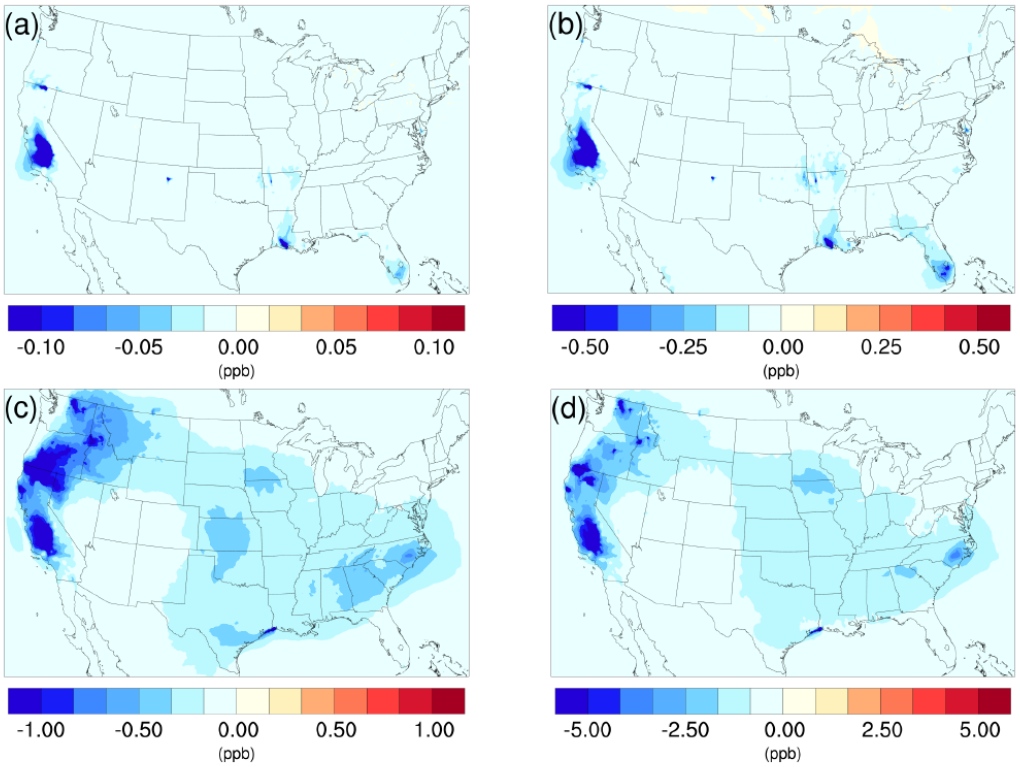

Figure S2. Spatial distribution of the difference in time-averaged NH_3 concentrations between the γ=10^{-5} case and the base case for (a) winter period, and (c) summer period and between the γ=10^{-4} case and the base case for (b) winter period and (d) summer period.

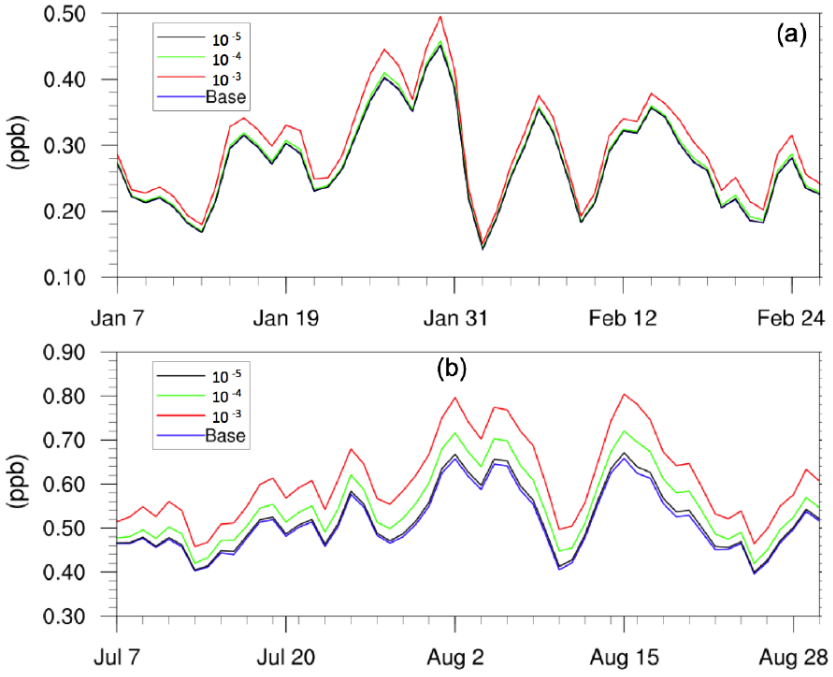

Figure S3. Daily, spatially-averaged HNO_3 concentrations for different scenarios for (a) winter period and (b) summer period

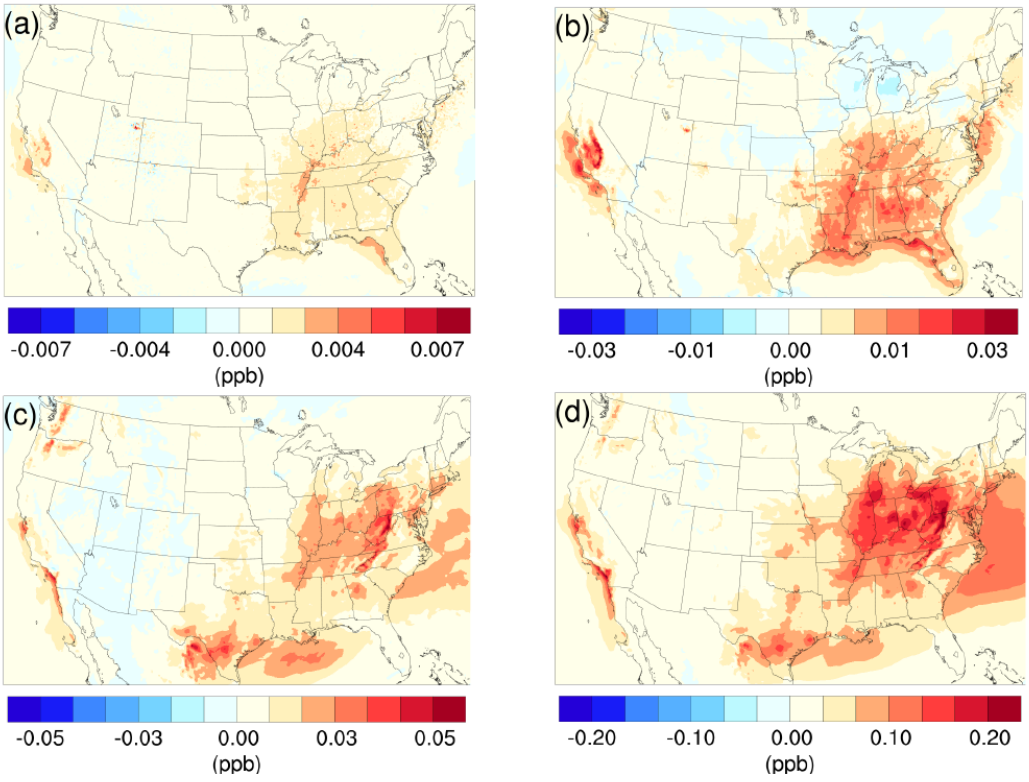

Figure S4. Spatial distribution of the difference in time-averaged HNO_3 concentrations between the γ=10^{-5} case and the base case for (a) winter period, and (c) summer period and between the γ=10^{-4} case and the base case for (b) winter period and (d) summer period.

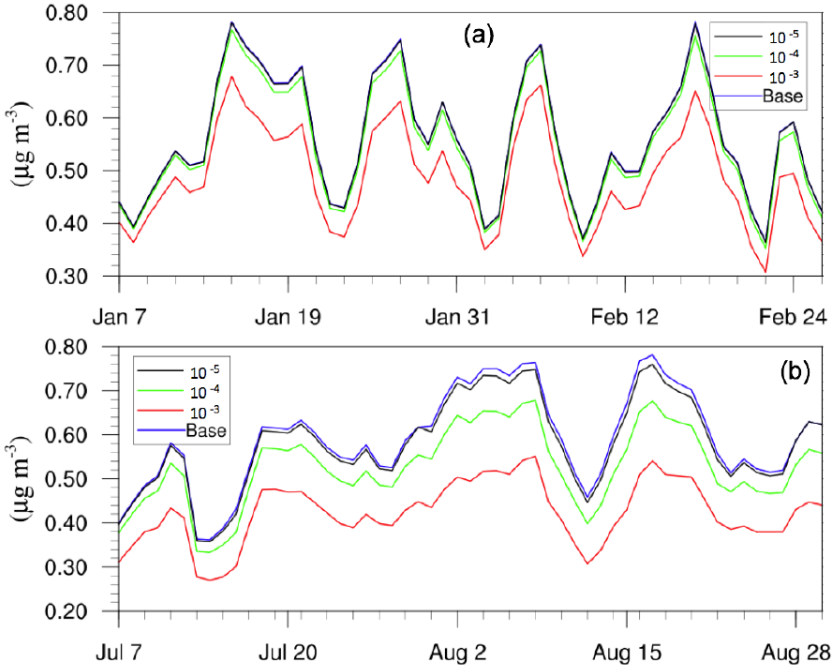

Figure S5. Daily, spatially-averaged NH_4^+ concentrations of different scenarios for (a) winter period, and (b) summer period

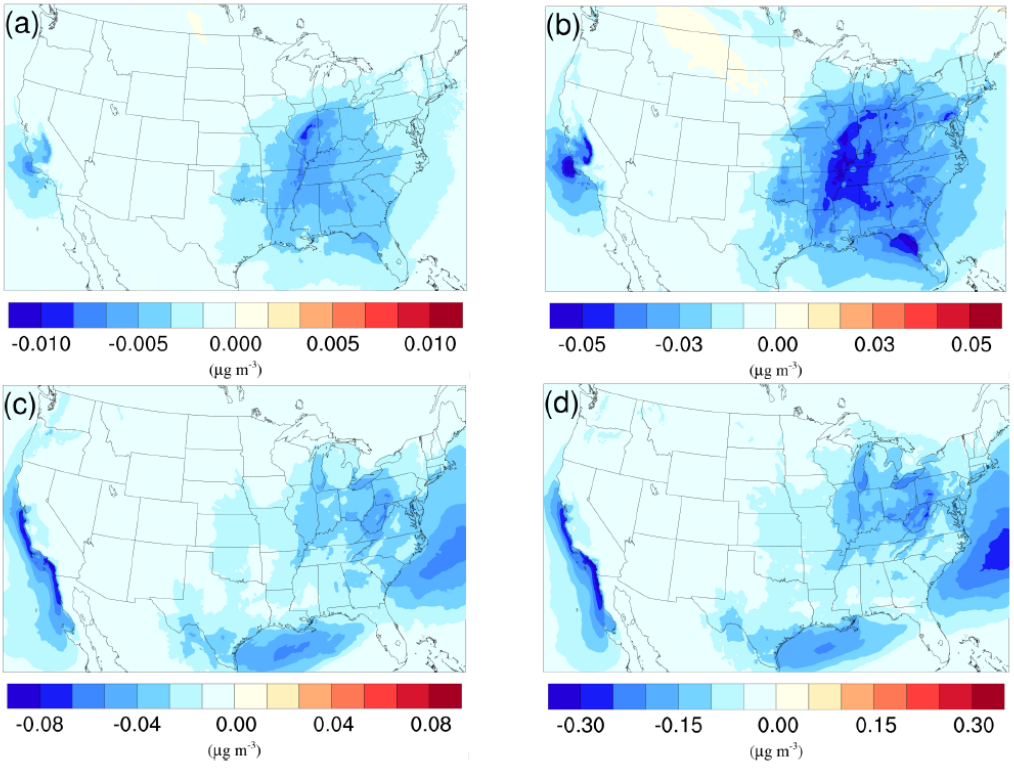

Figure S6. Spatial distribution of the difference in time-averaged NH_4^+ concentrations between the γ=10^{-5} case and the base case for (a) winter period and (c) summer period, and between the γ=10^{-4} case and the base case for (b) winter period and (d) summer period.

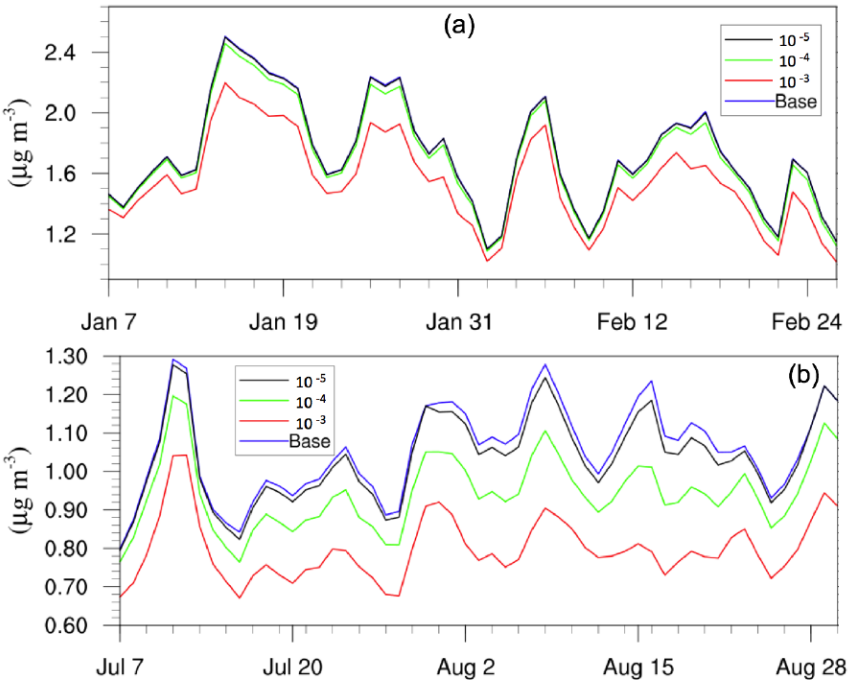

Figure S7. Daily, spatially-averaged NO_3^- concentrations of different scenarios for (a) winter period and (b) summer period

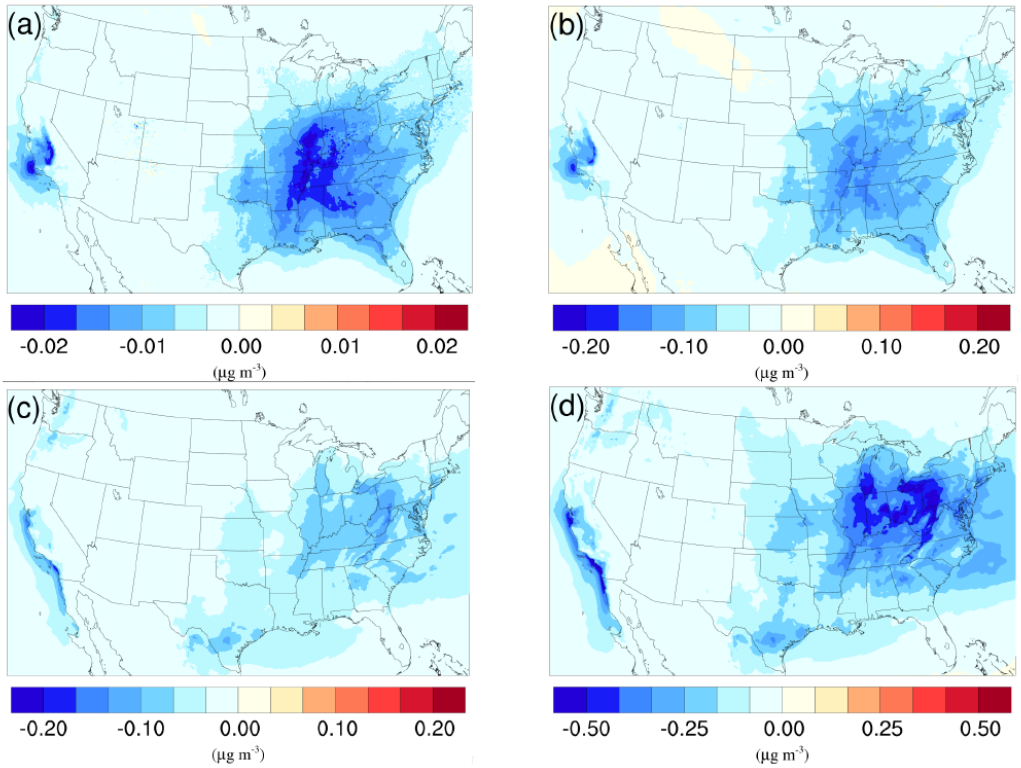

Figure S8. Spatial distribution of the difference in time-averaged NO_3^- concentrations between the γ=10^{-5} case and the base case for (a) winter period and (c) summer period and between the γ=10^{-4} case and the base case for (b) winter period and (d) summer period.

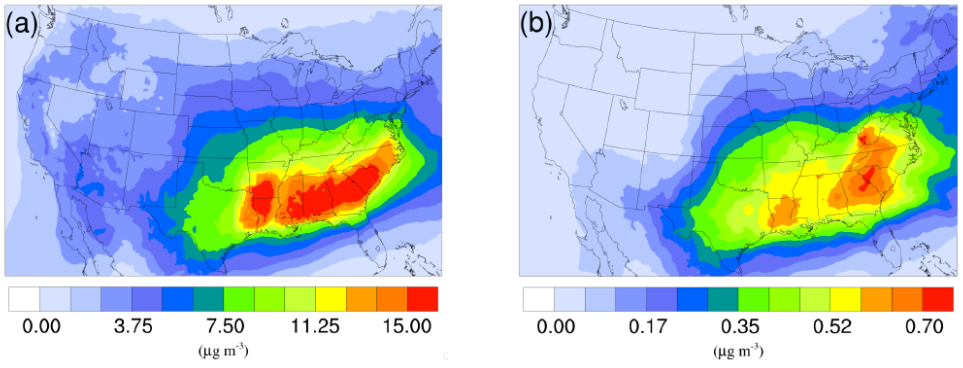

Figure S9. Spatial distribution of time-averaged (a) biogenic SOA concentrations, and (b) the isoprene epoxydiol derived SOA concentrations in the base case for the summer period.

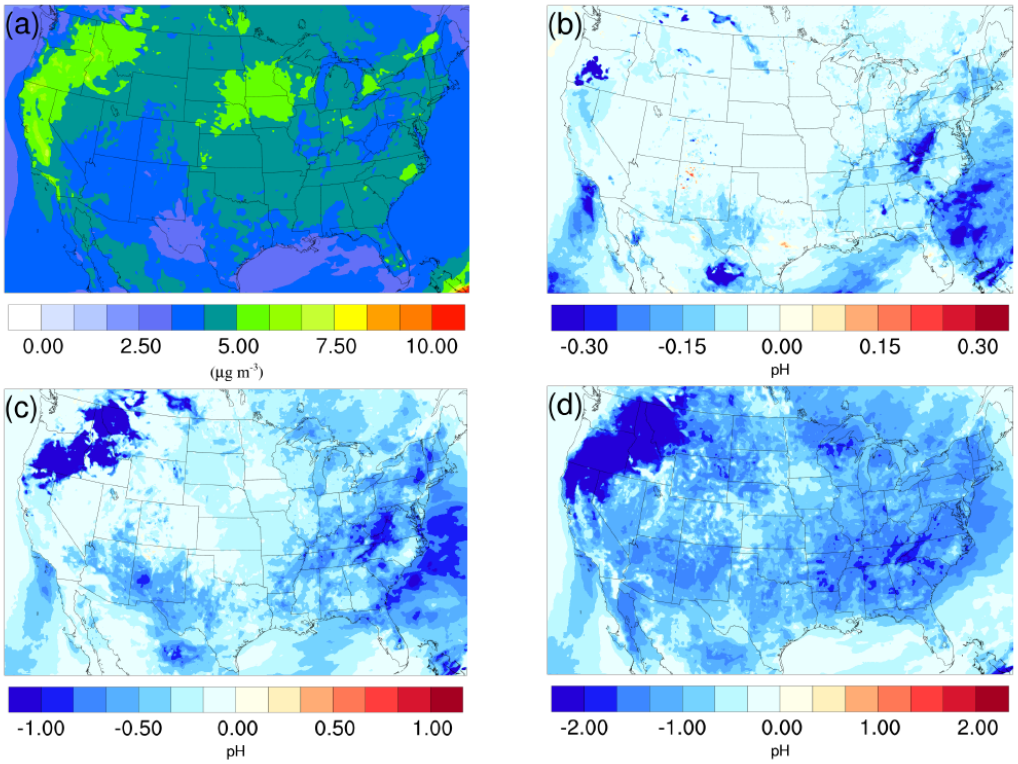

Figure S10. Spatial distribution of time-averaged (a) particle acidity (pH) in the base case for the summer period. Spatial distribution of the difference in time-averaged particle acidity between the γ=10^{-5} case and the base case, (c) γ=10^{-4} case and the base case, (d) γ=10^{-3} case and the base case during the summer period.

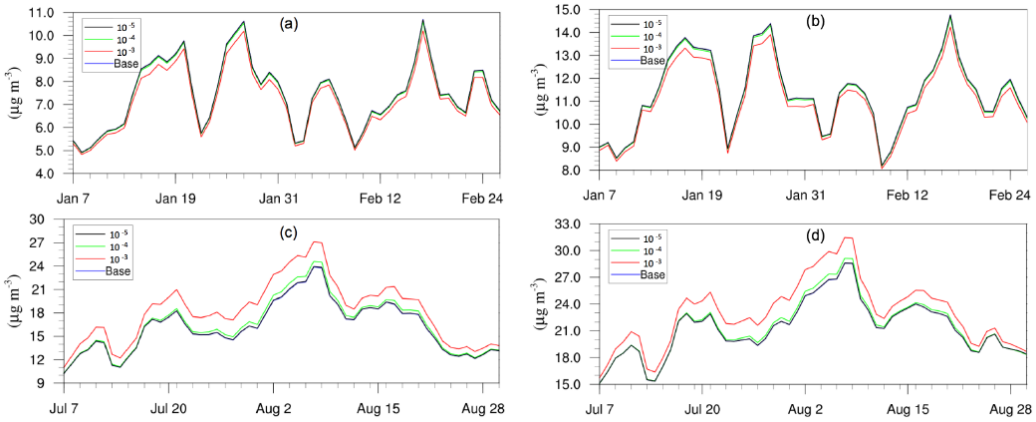

Figure S11. Daily, spatially-averaged concentrations of different scenarios for (a) $PM_{2.5}$ in winter, (b) PM_{10} in winter, (c) $PM_{2.5}$ in summer, and (d) PM_{10} in summer

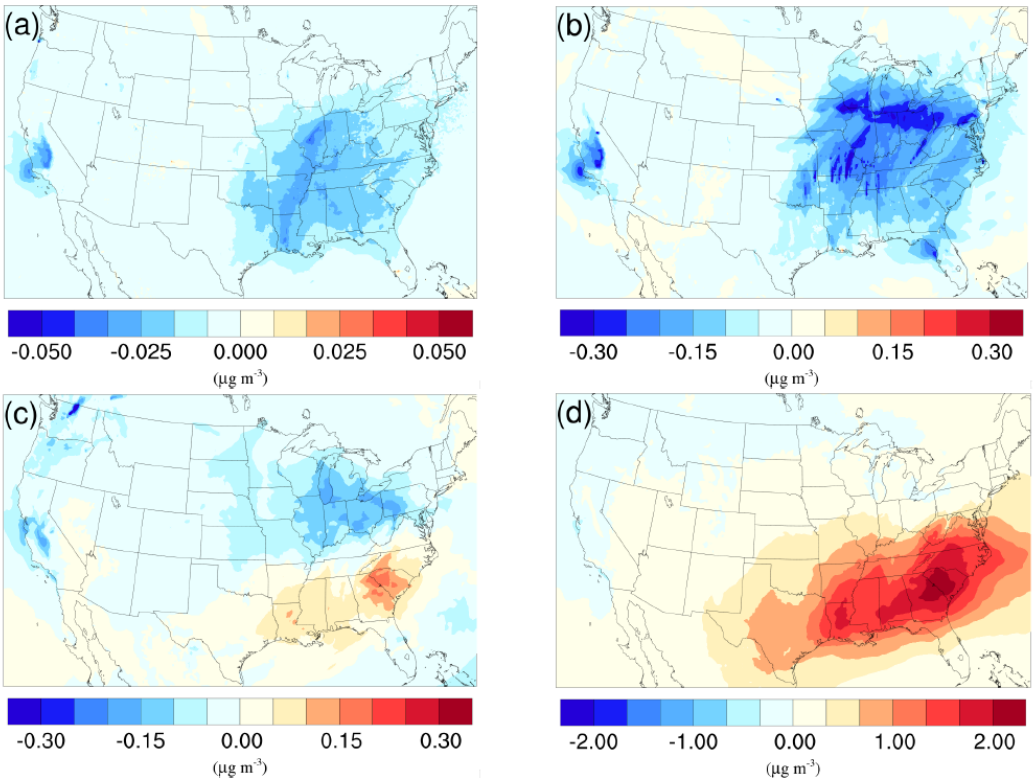

Figure S12. Spatial distribution of the difference in time-averaged $PM_{2.5}$ concentrations between the γ=10^{-5} case and the base case for (a) winter period and (c) summer period, and between the γ=10^{-4} case and the base case for (b) winter period and (d) summer period.